 CMES, vol.4, no.5, pp.603-618, 2003

3-D Transient Dynamic Crack Analysis by a Novel Time-Domain BEM [1]

Ch. Zhang[2] **and A. Savaidis**[3]

Abstract: A novel non-hypersingular time-domain traction BEM is presented for three-dimensional (3-D) transient elastodynamic crack analysis. The initial-boundary value problem is formulated as a set of non-hypersingular time-domain traction boundary integral equations (BIEs). To solve the time-domain traction BIEs, a time-stepping scheme based on the convolution quadrature formula of Lubich (1988a,b; 1994) for temporal discretization and a collocation method for spatial discretization is adopted. Numerical examples are given for an unbounded solid with a penny-shaped crack under a tensile and shear impact loading. A comparison of the present time-domain BEM with the conventional one shows that the novel time-domain method is much more stable and less sensitive to the choice of the used time-steps.

keyword: 3-D Time-domain boundary element method, Non-hypersingular boundary integral equations, Transient elastodynamic crack analysis, Elastodynamic stress intensity factors.

1 Introduction

The commonly applied time-domain BEM in elastodynamics suffers from the crucial choice of time-steps. The stability and the accuracy of the time-stepping method may be significantly influenced by the applied time-steps (Peirce and Seibrits, 1997; Frangi and Novati, 1999; Yu, Mansur, Carrer and Gong, 2000). A too small time-step may cause an instability in the numerical scheme, while a too large time-step may give rise to a strong numerical damping of the results. In recent years, several approaches have been proposed to improve the stability of the conventional time-domain BEM. Among them, the following methods should be mentioned:

- Method using higher order temporal shape functions (e.g., Wang, Wang and Liou, 1997);
- Half-step scheme using zeta-transform and variable time-steps (e.g., Peirce and Seibrits, 1997);
- Time weighting method (Yu, Mansur, Carrer and Gong, 1998a);
- Linear θ method (Yu, Mansur, Carrer and Gong, 1998b; Araujo, Mansur and Nishikava, 2000);
- Galerkin method (Yu, Mansur, Carrer and Gong, 2000);
- Method using "causal" shape functions (Frangi, 2000);
- Method using convolution quadrature formula of Lubich (Schanz and Antes, 1997a,b; Schanz, 1998; Gaul and Schanz, 1999; Zhang, 2000a,b; Zhang and Savaidis, 2000);
- Method using modified Green's functions (Coda and Venturini, 1996).

This paper presents an improved time-domain BEM for transient elastodynamic crack analysis. The present method applies the convolution quadrature formula of Lubich (1988a,b; 1994) for approximating the temporal convolution arising in the time-domain BIEs and the collocation method for the spatial discretization. Unlike the classical time-marching scheme frequently applied in the time-domain BEM, the convolution quadrature formula of Lubich (1988a,b;1994) bases on a multistep method and uses Laplace-domain Green's functions instead of time-domain Green's functions. For time-domain displacement BIEs, this method was successfully implemented by Schanz and Antes (1997a,b), Schanz (1998) and Gaul and Schanz (1999). Applications of the convolution quadrature method to time-domain traction BIEs

[1] This paper is dedicated to Prof. Dr.-Ing. G. Kuhn, University of Erlangen-Nürnberg, Germany, on the occasion of his 60th birthday.

[2] Department of Civil Engineering, Hochschule Zittau/Görlitz, University of Applied Sciences, D-02763 Zittau, Germany.

[3] Department of Mechanics, National Technical University of Athens, GR-15773 Athens, Greece.

for cracked solids were presented by Zhang (2000a,b) using a Galerkin method, and Zhang and Savaidis (2000c) using a collocation method for the spatial discretization of the traction BIEs.

A non-hypersingular time-domain traction boundary integral equation (BIE) formulation is used in the analysis. Though many alternative methods are available to derive non-hypersingular traction BIEs (e.g., Sládek and Sládek, 1984; Nishimura and Kobayashi, 1989; Tanaka, Sládek and Sládek, 1994; Aliabadi, 1997; Beskos, 1997; Bonnet, 1999; Chen, 1999; Tada, Fukuyama and Madariaga, 2000), a direct method using a two-state conservation law of elastodynamics (Zhang and Achenbach, 1989; Zhang, 1991; Zhang and Gross, 1992) is applied in the paper. For an unbounded solid with a crack, the unknown quantities of the non-hypersingular traction BIEs are the crack-opening-displacements (CODs) and their derivatives. The temporal convolution of the time-domain BIEs is approximated by the convolution quadrature formula of Lubich (1988a,b; 1994), while the spatial discretization of the BIEs is done by a collocation method. For the purpose of simplicity, two different spatial shape-functions for the CODs are adopted. While a "square-root" shape-function is used at the crack-front, a simple constant shape-function is applied for elements away from the crack-front. The use of the "square-root" shape-function takes the proper local behavior of the CODs at the crack-front into account and it permits a direct and accurate calculation of the elastodynamic stress intensity factors from the numerically computed CODs. To show the stability and the accuracy of the present method, numerical examples are presented for an unbounded 3-D solid containing a penny-shaped crack subjected to a tensile and shear impact loading. The most important advantage of the method over the conventional time-domain BEM is that the method is much more stable and less sensitive to the choice of the applied time-steps. Another advantage is that it can be easily extended to cases where the Laplace-domain Green's functions have closed or simpler forms than the corresponding time-domain Green's functions.

Non-hypersingular displacement gradient BEM for elastic and elastic/plastic stress analysis was presented by Okada, Rajiyah and Atluri (1988, 1989). A spectral scheme for dynamic fracture analysis of composites was developed by Hwang and Geubelle (2000). A 3-D time-domain BEM for dynamic analysis of uncracked anisotropic elastic solids was implemented by Kögl and Gaul (2000), who used the dual reciprocity BEM and the elastostatic Green's functions for anisotropic solids.

2 Problem statement and time-domain BIEs

We consider a crack of arbitrary shape contained in a 3-D homogeneous, isotropic and linearly elastic solid as shown in Fig. 1. The cracked solid satisfies the equations of motion (Achenbach, 1973)

$$\sigma_{ij,j} + \rho p_i = \rho \ddot{u}_i \,, \tag{1}$$

the Hooke's law

$$\sigma_{ij} = E_{ijkl} u_{k,l} \,, \tag{2}$$

the zero initial conditions

$$u_i(\mathbf{x},t) = \dot{u}_i(\mathbf{x},t) = 0 \,, \qquad \text{for} \quad t = 0 \,, \tag{3}$$

and the boundary conditions

$$f_i(\mathbf{x},t) = 0 \,, \qquad \mathbf{x} \in A_c \,, \tag{4}$$

$$f_i(\mathbf{x},t) = f_i^*(\mathbf{x},t) \,, \qquad \mathbf{x} \in A_\sigma \,, \tag{5}$$

$$u_i(\mathbf{x},t) = u_i^*(\mathbf{x},t) \,, \qquad \mathbf{x} \in A_u \,. \tag{6}$$

In Eqs. (1)-(6), σ_{ij}, u_i and p_i represent the stress, the displacement and the body force components, ρ denotes the mass density, E_{ijkl} is the elasticity tensor, $f_i(\mathbf{x},t) = \sigma_{ij}(\mathbf{x},t) n_j$ stands for the traction vector with n_j being the unit normal vector, $A_c = A_c^+ + A_c^-$ with "$\pm$" indicating the upper and the lower crack-surfaces, A_σ is the exterior boundary on which the traction components are specified whereas A_u is the exterior boundary where the displacements are prescribed. Here and throughout the analysis, the conventional summation rule over double indices is implied, a comma after a quantity designates partial differentiation of the quantity with respect to spatial variables, while superscript dots denote temporal derivatives of the quantity.

The initial-boundary value problem governed by Eqs. (1)-(6) can be described by a set of time-domain traction BIEs. To derive non-hypersingular time-domain traction BIEs, we use the following conservation integral of linear elastodynamics

$$\begin{aligned} J_k^D &= \int_A \left[\frac{1}{2} (\sigma_{mn} * u_{m,n} + \rho \ddot{u}_i * u_i) \delta_{jk} - \sigma_{ij} * u_{i,k} \right] n_j dS \\ &- \int_V \rho p_i * u_{i,k} dV = 0 \,, \end{aligned} \tag{7}$$

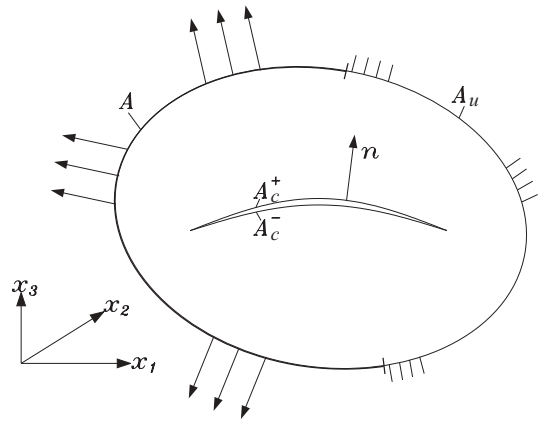

Figure 1 : A cracked 3-D solid

where A is the surface and V is the volume of a solid considered, n_j is the unit outward normal vector to A, and an asterisk $*$ denotes Riemann convolution which is defined by

$$f(t) = g(t) * h(t) = \int_0^t g(t-\tau)h(\tau)d\tau. \tag{8}$$

Note here that Eq. (7) is valid as long as the zero initial conditions (3) and no singularities within the considered solid are ensured.

We consider now two independent elastodynamic states in the same solid

$$\left\{u_i^{(1)}, \sigma_{ij}^{(1)}, p_i^{(1)}\right\}, \qquad \left\{u_i^{(2)}, \sigma_{ij}^{(2)}, p_i^{(2)}\right\}, \tag{9}$$

and require that both states satisfy the governing equations (1)–(2) and the zero initial conditions (3). According to the superposition principle, the sum of the two states

$$u_i = u_i^{(1)} + u_i^{(2)}, \quad \sigma_{ij} = \sigma_{ij}^{(1)} + \sigma_{ij}^{(2)}, \quad p_i = p_i^{(1)} + p_i^{(2)}, \tag{10}$$

satisfies the governing equations (1)–(2) and the zero initial conditions (3) too. Substitution of Eq. (10) into Eq. (7) leads to

$$\begin{aligned} J_k^D[u_i] &= J_k^D\left[u_i^{(1)}\right] + J_k^D\left[u_i^{(2)}\right] \\ &+ \int_A \left\{\varepsilon_{rst}\varepsilon_{rkj}\sigma_{ij}^{(2)} * u_{i,t}^{(1)} n_s - \left[\sigma_{ij}^{(1)} * u_{i,k}^{(2)}\right.\right. \\ &- \left.\left.\rho\ddot{u}_i^{(1)} * u_i^{(2)}\delta_{jk}\right] n_j\right\} dS \\ &- \rho\int_V \left[p_i^{(1)} * u_{i,k}^{(2)} + p_i^{(2)} * u_{i,k}^{(1)}\right] dV = 0. \end{aligned} \tag{11}$$

Since $u_i^{(1)}$ and $u_i^{(2)}$ are two distinct elastodynamic states which satisfy the governing equations (1)–(2) and the zero initial conditions (3), the first two terms in Eq. (11) vanish identically. Thus, a two-state conservation integral is obtained from Eq. (11) as

$$\begin{aligned} &\int_A \left\{\varepsilon_{rst}\varepsilon_{rkj}\sigma_{ij}^{(2)} * u_{i,t}^{(1)} n_s - \left[\sigma_{ij}^{(1)} * u_{i,k}^{(2)} - \rho\ddot{u}_i^{(1)} * u_i^{(2)}\delta_{jk}\right] n_j\right\} dS \\ &-\rho\int_V \left[p_i^{(1)} * u_{i,k}^{(2)} + p_i^{(2)} * u_{i,k}^{(1)}\right] dV = 0, \end{aligned} \tag{12}$$

in which ε_{rst} represents the permutation tensor.

Now state (1) is chosen as the actual unknown displacement and stress fields

$$\left\{u_i^{(1)}, \sigma_{ij}^{(1)}, \rho p_i^{(1)}\right\} = \left\{u_i, \sigma_{ij}, 0\right\}, \tag{13}$$

and state (2) is chosen as the fundamental solutions

$$\left\{u_i^{(2)}, \sigma_{ij}^{(2)}, \rho p_i^{(2)}\right\} = \left\{u_{ik}^G a_k, \sigma_{ijk}^G a_k, \delta(\mathbf{x}-\mathbf{y})\delta(t)a_i\right\}, \tag{14}$$

where u_{ik}^G and σ_{ijk}^G are the 3-D time-domain Green's functions for the uncracked full-space, a_k indicates the directions of the applied impulsive unit point force, and $\delta(\cdot)$ represents the Dirac delta. Substituting Eqs. (13) and (14) into Eq. (12) and using the sifting property of the Dirac delta, the volume integral in Eq. (12) can be evaluated analytically as

$$\rho\int_V \left[p_i^{(1)} * u_{i,k}^{(2)} + p_i^{(2)} * u_{i,k}^{(1)}\right] dV = u_{l,k}(\mathbf{x},t)a_l. \tag{15}$$

Eqs. (12) and (15) together result in a representation formula for the displacement gradients $u_{k,l}(\mathbf{x},t)$ as

$$\begin{aligned} u_{k,l}(\mathbf{x},t) &= -\int_A \left[\varepsilon_{rst}\varepsilon_{rlj}\sigma_{ijk}^G * u_{i,t} n_s\right. \\ &- \left.\left(u_{ik,l}^G * \sigma_{ij} - \rho u_{ik}^G * \ddot{u}_i\delta_{jl}\right) n_j\right] dS, \quad \mathbf{x} \notin A. \end{aligned} \tag{16}$$

Substituting Eq. (16) into Hooke's law (2), taking the limit procedure $\mathbf{x} \to A$, and considering the boundary conditions (4)-(6), we obtain the following non-hypersingular time-domain traction BIEs

$$-E_{pqkl} n_q(\mathbf{x}) \int_{A_c^+} \left(\varepsilon_{rst} \varepsilon_{rlj} \sigma^G_{ijk} * \Delta u_{i,t} n_s + \rho u^G_{ik} * \Delta \ddot{u}_i n_l \right) dS$$
$$-E_{pqkl} n_q(\mathbf{x}) \int_{A_\sigma + A_u} \Big[\varepsilon_{rst} \varepsilon_{rlj} \sigma^G_{ijk} * u_{i,t} n_s$$
$$- \left(u^G_{ik,l} * \sigma_{ij} - \rho u^G_{ik} * \ddot{u}_i \delta_{jl} \right) n_j \Big] dS = \delta_A f_p(\mathbf{x}, t), \quad \mathbf{x} \in A, \tag{17}$$

where the integrals are understood as Cauchy principal value integrals, $\delta_A = 1$ if $\mathbf{x} \in A_c^+$ while $\delta_A = 1/2$ when $\mathbf{x} \in A_\sigma + A_u$, and Δu_i are the crack-opening-displacements (CODs) defined by

$$\Delta u_i(\mathbf{y}, \tau) = u_i(\mathbf{y} \in A_c^+, \tau) - u_i(\mathbf{y} \in A_c^-, \tau). \tag{18}$$

It should be mentioned here that the time-domain traction BIEs (17) are non-hypersingular with the exception at the crack-front. Since an additional square-root singularity in the displacement gradients $\Delta u_{i,t}$ occurs at the crack-front, Eq. (17) represents a set of hypersingular BIEs when the collocation points are selected to be located at the crack-front.

For the sake of brevity and to show the essential features of the present numerical solution procedure, it suffices to consider the first integral over A_c^+ only, since the last integral over $A_\sigma + A_u$ has the same singularities as the first integral does. This can be best done by considering an unbounded 3-D solid. In this case, the last boundary integral of Eq. (17) vanishes and the time-domain traction BIEs (17) are simplified to

$$-E_{pqkl} n_q(\mathbf{x}) \int_{A_c^+} \left(\varepsilon_{rst} \varepsilon_{rlj} \sigma^G_{ijk} * \Delta u_{i,t} n_s + \rho u^G_{ik} * \Delta \ddot{u}_i n_l \right) dS$$
$$= f_p(\mathbf{x}, t), \qquad \mathbf{x} \in A_c^+. \tag{19}$$

The actual unknown quantities of the non-hypersingular time-domain traction BIEs (19) are the CODs and their derivatives. Once the CODs have been computed numerically by solving the non-hypersingular traction BIEs (19), the displacements at any interior points of the cracked solid can be calculated by using the following representation formula from the Betti-Rayleigh reciprocal theorem

$$u_k(\mathbf{x}, t) = \int_{A_c^+} \sigma^G_{ijk}(\mathbf{x}, t; \mathbf{y}, \tau) * \Delta u_i(\mathbf{y}, \tau) n_j dS, \quad \mathbf{x} \notin A_c^+, \tag{20}$$

while their gradients can be determined by using Eq. (16). The stress field can be obtained subsequently by using the Hooke's law (2). The elastodynamic stress intensity factors can be calculated directly from the CODs, as will be shown in section 4. Note here that the displacement gradients and the stresses at points very close to the boundaries of the cracked solid can be accurately determined by using Eq. (16) and Hooke's law.

3 Numerical solution procedure

A novel time-stepping method is adopted for solving the non-hypersingular time-domain traction BIEs (19) numerically. The method uses the convolution quadrature formula of Lubich (1988a,b; 1994) for temporal convolution and a collocation method for spatial discretization. The crack-surface A_c^+ is discretized into E quadrilateral elements, i.e.,

$$A_c^+ = \sum_{e=1}^{E} A_e^+, \tag{21}$$

and the unknown CODs Δu_i are approximated by the following interpolation functions

$$\Delta u_i(\mathbf{y}, \tau) = \sum_{e=1}^{E} \mu_e(\mathbf{y}) \eta_{i;e}(\tau), \tag{22}$$

where $\mu_e(\mathbf{y})$ is a spatial shape-function defined by

$$\mu_e(\mathbf{y}) = g(\mathbf{y}) H(\mathbf{y}) = \begin{cases} g(\mathbf{y}), & \mathbf{y} \in A_e^+, \\ 0, & \mathbf{y} \notin A_e^+, \end{cases} \tag{23}$$

and $\eta_{i;e}(\tau)$ is an unknown time function to be determined. In Eq. (23), $g(\mathbf{y})$ describes the spatial variation of Δu_i within the e-th element A_e^+, and $H(\mathbf{y})$ is the 3-D Heaviside function, see Appendix C.

Substituting Eq. (22) into the time-domain traction BIEs (19), using the convolution quadrature formula of Lubich

(1988a,b;1994), see Appendix A

$$f(t) = g(t) * h(t) = \int_0^t g(t-\tau)h(\tau)d\tau$$
$$\Longrightarrow \quad f(n\Delta t) = \sum_{j=0}^{n} \omega_{n-j}(\Delta t)h(j\Delta t)\,, \tag{24}$$

choosing E collocation points on A_c^+ and requiring that the BIEs (19) have to be satisfied at each collocation point $\mathbf{x}^d$ $(d = 1,2,...E)$, the non-hypersingular time-domain traction BIEs (19) are converted into a system of linear algebraic equations

$$\sum_{j=0}^{n}\sum_{e=1}^{E} A_{ip;ed}^{n-j}\eta_{i;e}^{j} = f_{p;d}^{n}, \qquad (n = 0,1,2,...,N; \quad d = 1,2,...,E)\,, \tag{25}$$

where the time variable t is divided into N equal time-steps Δt, i.e. $t = \sum_{n=0}^{N}\Delta t$. The system matrix $A_{ip;ed}^{n-j}$ and the right-hand side $f_{p;d}^{n}$ of Eq. (25) are given by

$$A_{ip;ed}^{n-j} = \frac{r^{-(n-j)}}{M}\sum_{m=0}^{M-1}\hat{A}_{ip;ed}(p_m)e^{-2\pi i(n-j)m/M}\,, \tag{26}$$

$$f_{p;d}^{n} = f_p(\mathbf{x}^d, n\Delta t)\,, \tag{27}$$

in which

$$p_m = \frac{\delta(\zeta_m)}{\Delta t}, \quad \delta(\zeta_m) = \sum_{j=1}^{2}\frac{(1-\zeta_m)^j}{j}, \quad \zeta_m = re^{2\pi i\cdot m/M}\,. \tag{28}$$

The numerical error in computing $A_{ip;ed}^{n-j}$ using the convolution quadrature formula of Lubich (1988a,b;1994) is of the order $O(\sqrt{\varepsilon})$ when $M = N$ and $r^N = \sqrt{\varepsilon}$ are selected. Here, ε is the numerical error arised in the computation of the Laplace-transform of the system matrix $\hat{A}_{ip;ed}(p_m)$, which corresponds to the integration weights $\omega_{n-j}(\Delta t)$ of the convolution quadrature formula (24). The system matrix in the Laplace-domain has the following form

$$\hat{A}_{ip;ed}(p_m) = -E_{pqkl}n_q(\mathbf{x}^d)\left[\varepsilon_{rst}\varepsilon_{rlj}\int_{A_e^+}\hat{\sigma}_{ijk}^{G}\left(g_{,t}+gH_{,t}\right)n_s dS + \rho p_m^2\int_{A_e^+}\hat{u}_{ik}^{G}gn_l dS\right], \tag{29}$$

where $\hat{u}_{ik}^{G}$ and $\hat{\sigma}_{ijk}^{G}$ represent the displacement and the stress Laplace-domain Green's functions which are given in Appendix B. A special feature of the present time-domain BEM is that it applies Laplace-domain instead of time-domain Green's functions. The method is advantageous for cases where the Laplace-domain Green's functions have closed or simpler forms than their corresponding time-domain Green's functions. The system matrix defined by Eq. (26) is real-valued and it can be evaluated very efficiently by using the Fast Fourier Transform (FFT).

For planar cracks whose surfaces lie in the $x_1 - x_2$–plane, Eq. (29) can be recast into the following form

$$\begin{aligned}\hat{A}_{ip;ed}(p_m) &= E_{p3kl}\left\{\varepsilon_{r3\alpha}\varepsilon_{rlj}\int_{A_e^+}\hat{\sigma}_{ijk}^{G}(\mathbf{x}^d;\mathbf{y})g_{,\alpha}(\mathbf{y})dS\right.\\ &+ \left.\varepsilon_{r3\alpha}\varepsilon_{rlj}\int_{A_e^+}\hat{\sigma}_{ijk}^{G}(\mathbf{x}^d;\mathbf{y})g(\mathbf{y})H_{,\alpha}(\mathbf{y})dS\right\}\\ &+ \rho p_m^2 E_{p3k3}\int_{A_e^+}\hat{u}_{ik}^{G}(\mathbf{x}^d;\mathbf{y})g(\mathbf{y})dS\,.\end{aligned} \tag{30}$$

By invoking the property of the 3-D Heaviside function (Appendix C) the second integral on the right-hand side of Eq. (30) can be transformed into a line integral as

$$\int_{A_e^+}\hat{\sigma}_{ijk}^{G}(\mathbf{x}^d;\mathbf{y})g(\mathbf{y})H_{,\alpha}(\mathbf{y})dS = -\int_{\partial A_e^+}\hat{\sigma}_{ijk}^{G}(\mathbf{x}^d;\mathbf{y})g(\mathbf{y})m_\alpha(\mathbf{y})ds\,, \tag{31}$$

where $\mathbf{m} = \mathbf{t}\times\mathbf{n}$ is the unit vector normal to ∂A_e^+ tangent to A_e^+ and pointing outward, and $\mathbf{t}$ is the unit tangent vector to ∂A_e^+, see Fig. 2. With Eq. (31), Eq. (30) can be rewritten as

$$\begin{aligned}\hat{A}_{ip;ed}(p_m) &= E_{p3kl}\left\{\varepsilon_{r3\alpha}\varepsilon_{rlj}\int_{A_e^+}\hat{\sigma}_{ijk}^{G}(\mathbf{x}^d;\mathbf{y})g_{,\alpha}(\mathbf{y})dS\right.\\ &- \left.\varepsilon_{r3\alpha}\varepsilon_{rlj}\int_{\partial A_e^+}\hat{\sigma}_{ijk}^{G}(\mathbf{x}^d;\mathbf{y})g(\mathbf{y})m_\alpha(\mathbf{y})ds\right\}\\ &+ \rho p_m^2 E_{p3k3}\int_{A_e^+}\hat{u}_{ik}^{G}(\mathbf{x}^d;\mathbf{y})g(\mathbf{y})dS\,.\end{aligned} \tag{32}$$

In the case of $e \neq d$, i.e., $\mathbf{x}^d \neq \mathbf{y}$, all integrals in Eq. (32) are regular and they can be integrated numerically by using standard Gaussian quadrature formula. For $e = d$, the second integral of Eq. (32) is still regular since $\mathbf{x}^d$ is chosen to be at the centroid, i.e., off the boundary of the e-th patch ∂A_e^+. However, the first integral of Eq. (32) has a strong singularity of the order $O(1/r^2)$ while the last integral has a weak singularity of the order $O(1/r)$ at $r = 0$. Therefore, careful analytical or numerical treatments are required for evaluating these two integrals. To reduce the strong singularity $O(1/r^2)$, the first integral is rewritten as

$$\begin{aligned}
&\int_{A_e^+} \hat{\sigma}^G_{ijk}(\mathbf{x}^d;\mathbf{y}) g_{,\alpha}(\mathbf{y}) dS \\
&\quad = \int_{A_e^+} \hat{\sigma}^G_{ijk}(\mathbf{x}^d;\mathbf{y}) \left[g_{,\alpha}(\mathbf{y}) - g_{,\alpha}(\mathbf{x}^d) \right] dS \\
&\quad + g_{,\alpha}(\mathbf{x}^d) \int_{A_e^+} \hat{\sigma}^G_{ijk}(\mathbf{x}^d;\mathbf{y}) dS . \qquad (33)
\end{aligned}$$

By using Hooke's law

$$\hat{\sigma}^G_{ijk} = E_{ijuv} \hat{u}^G_{uk,v} , \qquad (34)$$

and the divergence theorem the last integral on the right-hand side of Eq. (33) can be transformed into a line integral as

$$\int_{A_e^+} \hat{\sigma}^G_{ijk}(\mathbf{x}^d;\mathbf{y}) dS = E_{ijuv} \int_{\partial A_e^+} \hat{u}^G_{uk}(\mathbf{x}^d;\mathbf{y}) m_v(\mathbf{y}) ds . \qquad (35)$$

The integral on the right-hand side of Eq. (35) is again regular since $\mathbf{x}^d$ is located off the boundary of the e-th patch, i.e., $\mathbf{x}^d \notin \partial A_e^+$. Substitution of Eqs. (33) and (35) into Eq. (32) provides

$$\begin{aligned}
\hat{A}_{ip;ed}(p_m) &= E_{p3kl} \left\{ \varepsilon_{r3\alpha} \varepsilon_{rlj} \int_{A_e^+} \hat{\sigma}^G_{ijk}(\mathbf{x}^d,\mathbf{y}) \times \right. \\
&\qquad \left[g_{,\alpha}(\mathbf{y}) - g_{,\alpha}(\mathbf{x}^d) \right] dS \\
&+ \varepsilon_{r3\alpha} \varepsilon_{rlj} E_{ijuv} g_{,\alpha}(\mathbf{x}^d) \int_{\partial A_e^+} \hat{u}^G_{uk}(\mathbf{x}^d,\mathbf{y}) m_v(\mathbf{y}) ds \\
&- \left. \varepsilon_{r3\alpha} \varepsilon_{rlj} \int_{\partial A_e^+} \hat{\sigma}^G_{ijk}(\mathbf{x}^d,\mathbf{y}) g(\mathbf{y}) m_\alpha(\mathbf{y}) ds \right\} \\
&+ \rho p_m^2 E_{p3k3} \int_{A_e^+} \hat{u}^G_{ik}(\mathbf{x}^d,\mathbf{y}) g(\mathbf{y}) dS . \qquad (36)
\end{aligned}$$

For $e \neq d$, all integrals in Eq. (36) are regular and they can be integrated numerically by using standard Gaussian quadrature formula. For $e = d$, the first integral of Eq. (36) has a weak singularity of the order $O(1/r)$ due to the following asymptotics

$$\begin{aligned}
&\hat{\sigma}^G_{ijk}(\mathbf{x}^d,\mathbf{y}) = O(1/r^2) , \qquad \mathbf{y} \to \mathbf{x}^d , \\
&g_{,\alpha}(\mathbf{y}) - g_{,\alpha}(\mathbf{x}^d) = O(r) , \qquad \mathbf{y} \to \mathbf{x}^d , \qquad (37)
\end{aligned}$$

where use is made of the Hölder continuity condition of $g_{,\alpha}$ at $\mathbf{x}^d$. The last integral of Eq. (36) has the same weak singularity of the order $O(1/r)$ as the first integral does. To handle the weak singularity $O(1/r)$, a quadrilateral element is divided into four triangular sub-elements and subsequently a coordinate transform from Cartesian into polar coordinate system (r,ϕ) with the origin at $\mathbf{x}^d$ is applied where

$$y_1 - x_1^d = r\cos\phi , \quad y_2 - x_2^d = r\sin\phi , \quad y_3 = x_3^d = 0 . \qquad (38)$$

This transformation results in

$$dS = r dr d\phi . \qquad (39)$$

The r term in Eq. (39) cancels the $1/r$ term arising in the first and the last integrals of (36). Hence, the weakly singular integrals of Eq. (39) after the coordinate transform are regular and they can be integrated numerically by using standard Gaussian quadrature formula. To avoid possible cancellations in the term $[\exp(-k_T r)/r - \exp(-k_L r)/r]$ appearing in Laplace-domain Green's functions for small values of $k_T r$ or $k_L r$, the series expansions of the Laplace-domain Green's functions are used, see Appendix B for more details.

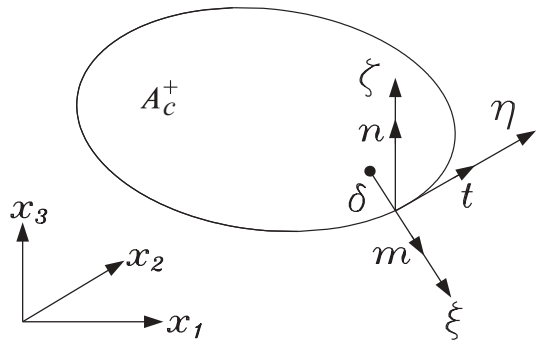

Figure 2 : A 3-D crack in local and global coordinate systems

For the purpose of simplicity, two simple spatial shape-functions are applied in the present analysis. For elements away from the crack-front, $g(\mathbf{y})$ is taken to be constant (constant element), while for elements in the first two rows behind the crack-front a "square-root" shape function is adopted to describe the proper local behavior of the CODs near the crack-front. The use of "square-root" shape function in the second row behind the crack-front as "transition elements" improves the accuracy of the present numerical solution procedure for computing the elastodynamic stress intensity factors. Note here that for 3-D planar cracks two uncoupled sets of BIEs are obtained: one for the normal COD Δu_3 and the other for the transverse CODs Δu_α.

It should be remarked here that the Hölder continuity condition, i.e., the CODs must be $C^{1,\alpha}$ continuous, which is required by the first integral of Eq. (36), is ensured in the present numerical solution procedure, since the collocation points are chosen to be located at the elements center and do not lie on the crack-front where the CODs are no longer $C^{1,\alpha}$ continuous. If higher order spatial shape-functions are used, the collocation points should be selected off the crack-front where the Hölder condition is violated. This can be done by either using discontinuous elements or using continuous elements with collocation points chosen at interior element nodes near the crack-front.

Note also that to compute the last term in Eq. (19) containing the double temporal derivatives of the CODs, i.e., $\Delta\ddot{u}_i$, the following convolution quadrature formula (see Appendix A) is used

$$f(t) = g(t) * \ddot{h}(t) = \ddot{g}(t) * h(t) = \int_0^t \ddot{g}(t-\tau)h(\tau)d\tau$$

$$\Longrightarrow \quad f(n\Delta t) = \sum_{j=0}^{n} \ddot{\omega}_{n-j}(\Delta t)h(j\Delta t)\,, \tag{40}$$

where

$$\ddot{\omega}_{n-j}(\Delta t) = \frac{r^{-(n-j)}}{M}\sum_{m=0}^{M-1} p_m^2 \hat{g}(p_m)e^{-2\pi i(n-j)m/M}. \tag{41}$$

An alternative way for evaluating the weights $\ddot{\omega}_{n-j}(\Delta t)$ instead of using Eq. (41) is the application of the following formula (Lubich, 2000)

$$\ddot{\omega}_{n-j}(\Delta t) = (\Delta t)^{-2}\sum_{k=0}^{4} \delta_k^{(2)}\omega_{n-j-k}(\Delta t)\,, \tag{42}$$

in which

$$\omega_{n-j-k}(\Delta t) = \frac{r^{-(n-j-k)}}{M}\sum_{m=0}^{M-1} \hat{g}(p_m)e^{-2\pi i(n-j-k)m/M}, \tag{43}$$

$\delta_k^{(2)}$ is determined by the equation

$$\sum_{k=0}^{4} \delta_k^{(2)}\zeta^k = \delta^2(\zeta)\,, \tag{44}$$

and $\delta(\zeta)$ is given in Eq. (28). Both methods are tested numerically by the present authors, and no remarkable differences in the numerical results were found. Therefore, only the first way by using Eq. (41) is presented here.

By considering the zero initial conditions (3) the following time-stepping scheme is obtained from Eq. (25)

$$\eta_{i;e}^n = \sum_{d=1}^{E}\left(A_{ip;ed}^0\right)^{-1}\left[f_{p;d}^n - \sum_{j=1}^{n-1}\sum_{f=1}^{E} A_{kp;df}^{n-j}\eta_{k;f}^j\right],$$

$$(n = 1,2,...,N)\,, \tag{45}$$

where $(A_{ip;ed}^0)^{-1}$ denotes the inverse matrix of $A_{ip;ed}^0$ at the time-step $n = 0$. The unknown time-dependent coefficients $\eta_{i;e}^n$ can be obtained by solving Eq. (45) time-step by time-step .

4 Numerical results and discussions

In this section, numerical results for the elastodynamic stress intensity factors will be presented to show the efficiency and the accuracy of the present time-domain traction BEM. The elastodynamic stress intensity factors are computed from the numerically calculated CODs by using the following relations

$$\begin{Bmatrix} K_I(t) \\ K_{II}(t) \\ K_{III}(t) \end{Bmatrix} = \frac{\mu\sqrt{2\pi}}{4(1-\nu)}\lim_{\delta\to 0}\frac{1}{\sqrt{\delta}}\begin{Bmatrix} \Delta u_\zeta(\delta,t) \\ \Delta u_\xi(\delta,t) \\ (1-\nu)\Delta u_\eta(\delta,t) \end{Bmatrix}, \tag{46}$$

with $K_I(t)$, $K_{II}(t)$ and $K_{III}(t)$ being the time-dependent mode-I, mode-II and mode-III elastodynamic stress intensity factors representing the strength of the inverse square-root singularity of the stress field at the crack-front, ν being the Poisson's ratio, Δu_ξ, Δu_η and Δu_ζ being the CODs in the local coordinate system, and δ being

a small distance of a point on the crack surface to the crack-front, see Fig. 2. The CODs Δu_ξ, Δu_η and Δu_ζ are computed at nodes nearest and with the shortest distance δ to the crack-front.

As a test example, a penny-shaped crack subjected to a separate tensile and shear impact loading is considered, see Fig. 3. Poisson's ratio is taken as $\nu = 0.29$, and a total number of 104 elements is used, see Fig. 4. For computing the system matrix by using Eq. (26) the relation $r^N = \sqrt{\varepsilon}$ with $\varepsilon = 10^{-12}$ has been applied. For convenience, the dynamic stress intensity factors $K_i(t)$ $(i = I, II, III)$ are normalized by their corresponding static values K_i^{st} as

$$\overline{K}_I(t) = \frac{K_I(t)}{K_I^{st}}, \quad K_I^{st} = \frac{2}{\pi}\sigma^* \sqrt{\pi a}, \tag{47}$$

$$\overline{K}_{II}(t) = \frac{K_{II}(t)}{K_{II}^{st}(\theta = 0^\circ)}, \quad K_{II}^{st} = \frac{4}{\pi(2-\nu)}\tau^* \sqrt{\pi a}\cos\theta, \tag{48}$$

$$\overline{K}_{III}(t) = \frac{K_{III}(t)}{K_{III}^{st}(\theta = 90^\circ)}, \quad K_{III}^{st} = -\frac{4(1-\nu)}{\pi(2-\nu)}\tau^* \sqrt{\pi a}\sin\theta, \tag{49}$$

where σ^* and τ^* are the amplitudes of the impact loading.

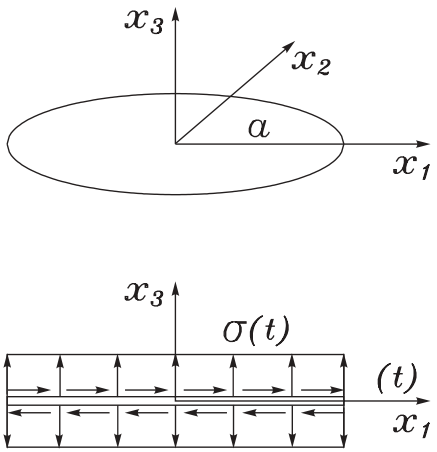

Figure 3 : A penny-shaped crack

For a pure tensile impact loading $\sigma_{33} = \sigma(t) = \sigma^* H(t)$ the problem is axissymmetric. Hence, $\overline{K}_{II}(t) = \overline{K}_{III}(t) = 0$ and $\overline{K}_I(t)$ is independent of the polar angle θ. Fig. 5 shows the normalized mode I dynamic stress intensity factor $\overline{K}_I(t)$ versus the dimensionless time $c_T t/a$, where c_T is the velocity of the transverse shear wave. A comparison of the present numerical result with that obtained via a conventional time-domain BEM developed by Zhang and Gross (1993) shows very good agreement. Here, the same time-step $c_T \Delta t/a = 0.2$ and the same mesh as shown in Fig. 4 have been used. Another check on the present time-domain BEM is made by comparing the numerical result at large $c_T t/a$ with its corresponding static value, and it is found that the deviation between them is less than 1%.

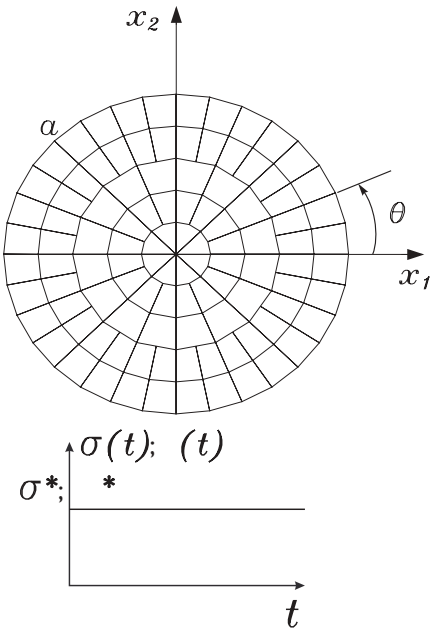

Figure 4 : BEM mesh and impact loading

The influences of the applied time-steps on the normalized dynamic stress intensity factor $\overline{K}_I(t)$ are shown in Figs. 6 and 7. Results presented in Fig. 6 are obtained by the conventional time-domain BEM of Zhang and Gross (1993), while Fig. 7 presents the corresponding numerical results provided by the novel time-domain BEM. Fig. 6 shows that the conventional time-stepping scheme cannot provide stable numerical results for the time-steps $c_T \Delta t/a = 0.1$ and $c_T \Delta t/a = 0.05$. For a large time-step $c_T \Delta t/a = 0.4$, the conventional time-stepping scheme causes an unreasonably large numerical damping which reveals that the conventional time-stepping method is inaccurate for large time-steps. In contrast, the present time-domain BEM is highly stable, even for quite

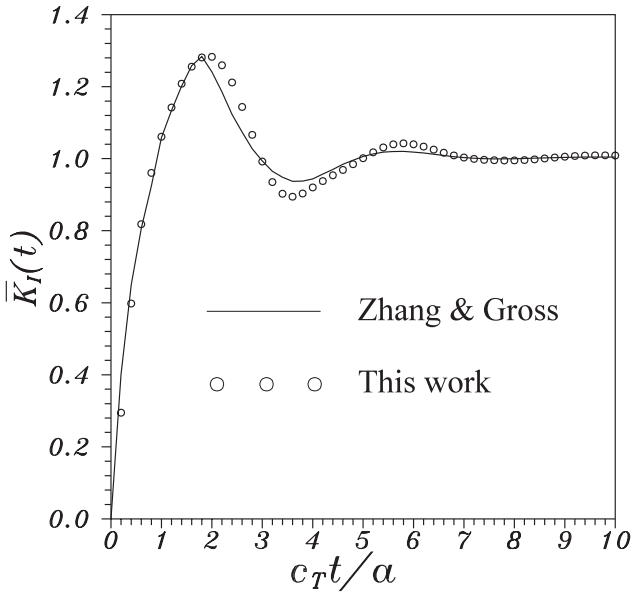

Figure 5 : The normalized $\overline{K}_I(t)$-factor versus $c_T t/a$

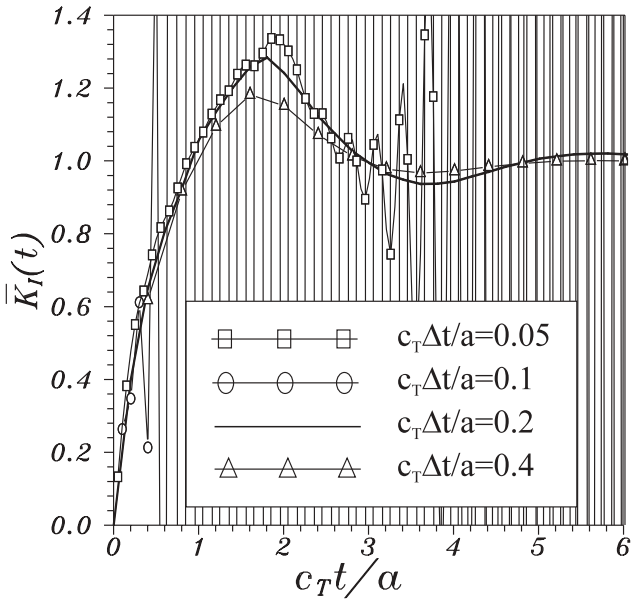

Figure 6 : Influences of time-steps on $\overline{K}_I(t)$ (Conventional time-domain method)

small time-steps $c_T\Delta t/a = 0.1$ and $c_T\Delta t/a = 0.05$. In the case of a large time-step $c_T\Delta t/a = 0.4$, the numerical damping arised in the novel time-domain method is much smaller than in the conventional time-domain method as shown in Fig. 6. Figs. 6 and 7 indicate clearly that the present time-domain BEM is pretty insensitive to the selected time-steps. This is an essential advantage of the present method over the conventional time-domain BEM

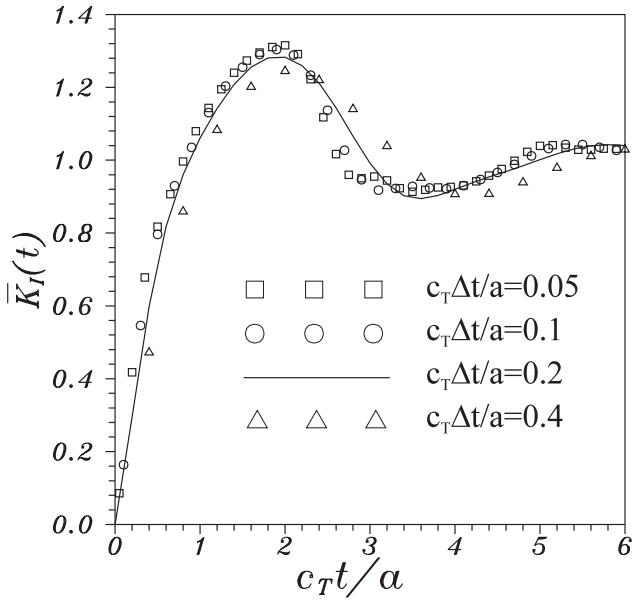

Figure 7 : Influences of time-steps on $\overline{K}_I(t)$ (Novel time-domain method)

using time-domain Green's functions.

For a pure shear impact loading $\sigma_{13} = \tau(t) = \tau^* H(t)$, $\overline{K}_I(t) = 0$ and the normalized dynamic stress intensity factors $\overline{K}_{II}(t)$ and $\overline{K}_{III}(t)$ are presented in Fig. 8, versus the dimensionless time $c_T t/a$ and the polar angle θ. It can be seen on Fig. 8 that the transient dynamic effect is confined to a small-time range. As the time increases, the dynamic stress intensity factors tend to their corresponding static values. In all cases considered here, a dynamic overshoot in the elastodynamic stress intensity factors is observed. The normalized dynamic stress intensity factors $\overline{K}_{II}(t)$ at $\theta = 0^\circ$ and $\overline{K}_{III}(t)$ at $\theta = 90^\circ$ along with the corresponding numerical results obtained by the conventional time-domain BEM of Zhang and Gross (1993) are given in Figs. 9 and 10 for the comparison purpose. Here again, a time-step $c_T\Delta t/a = 0.2$ and the same mesh as shown in Fig. 4 have been used in both numerical calculations. Though some discrepancies are observed in the normalized $\overline{K}_{II}(t)$ factor near its peak value, the overall agreement between both results are very satisfactory, at least for the selected time-step $c_T\Delta t/a = 0.2$.

Finally, Fig. 11 shows a comparison of the analytical static stress intensity factors and the numerically computed dynamic stress intensity factors at $c_T t/a = 10$. An excellent agreement between the analytical results and the numerical results of the present time-domain BEM is

obtained. This additional check confirms again the high accuracy of the novel time-domain BEM.

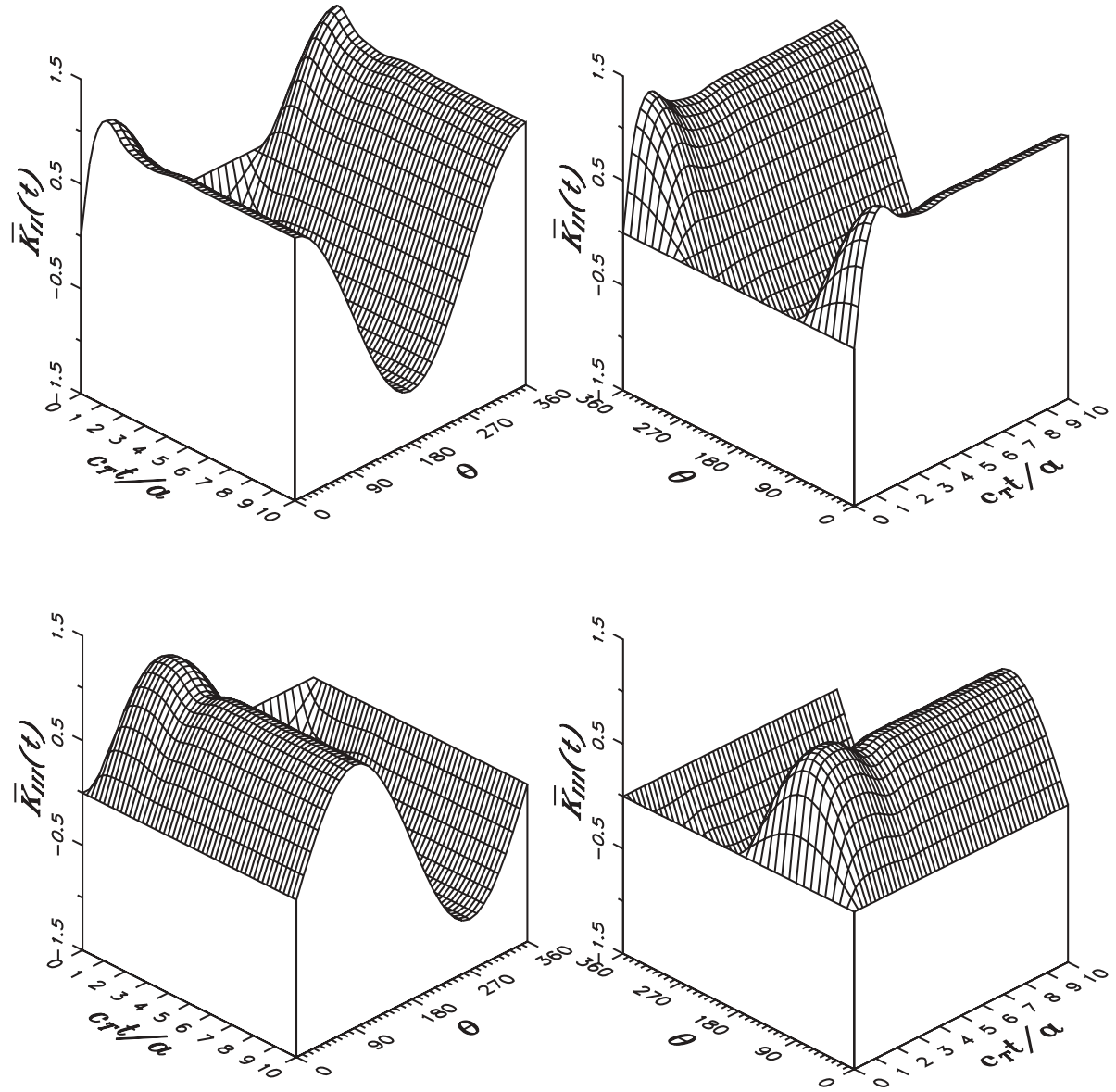

Figure 8 : Normalized $\overline{K}_{II}(t)$ and $\overline{K}_{III}(t)$ factors

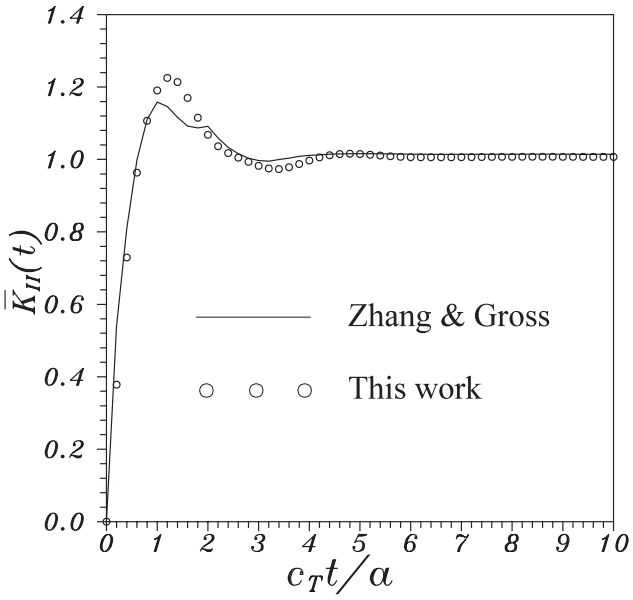

Figure 9 : Normalized $\overline{K}_{II}(t)$ factor ($\theta = 0^\circ$)

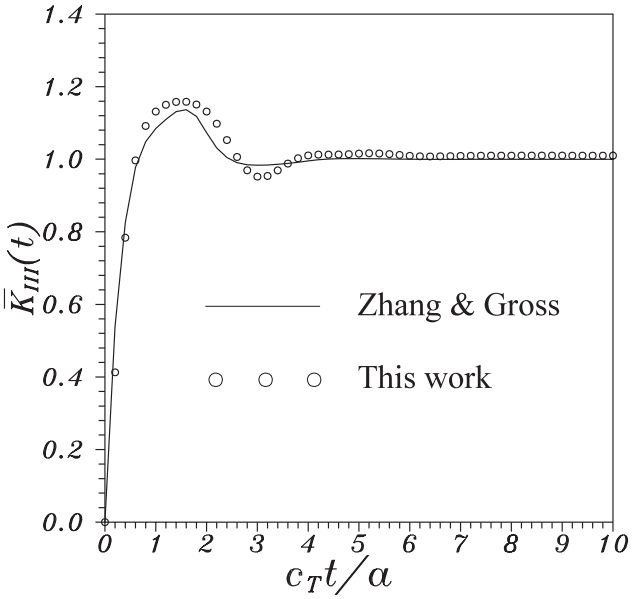

Figure 10 : Normalized $\overline{K}_{III}(t)$ factor ($\theta = 90^\circ$)

5 Conclusions

A novel non-hypersingular time-domain traction BEM is presented in this paper. Unlike the conventional time-domain BEM, the present method applies the convolution quadrature formula of Lubich (1988a,b; 1994) for approximating the temporal convolution and a collocation method for spatial discretization of the time-domain BIEs. A special feature of the present method

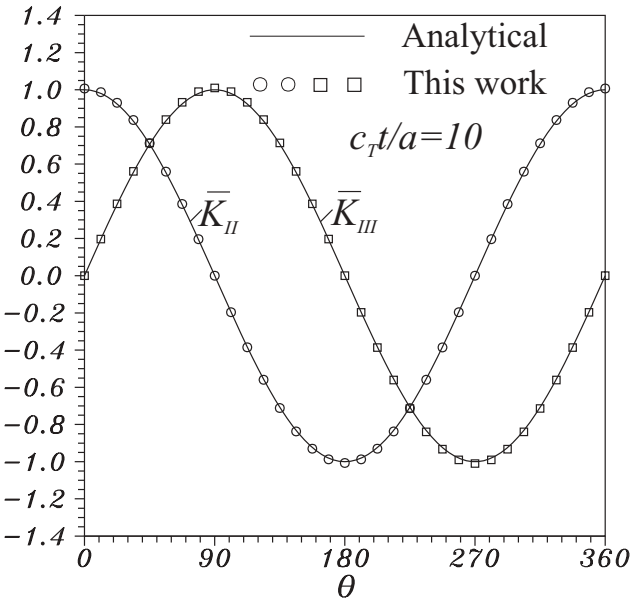

Figure 11 : Comparison of $\overline{K}_{II}(\theta = 0^\circ)$ and $\overline{K}_{III}(\theta = 90^\circ)$ factors at $c_T t/a = 10$ with analytical static results

is that its formulation is in the time-domain but it requires only Laplace-domain Green's functions instead of time-domain Green's functions. The most important advantage of the present time-domain BEM over the conventional time-domain BEM is that the method is much more stable and less sensitive to the choice of the selected time-steps. Another advantage of the method lies in its efficiency for cases where the Laplace-domain Green's functions have closed or simpler forms than their corresponding time-domain Green's functions.

Acknowledgement: The authors are grateful to Prof. Dr. C. Lubich, Institute of Mathematics, University of Tübingen, Germany, for many useful discussions on his convolution quadrature formula.

References

Achenbach, J. D. (1973): *Wave propagation in elastic solids*. North-Holland, Amsterdam/New York.

Aliabadi, M. H. (1997): Boundary element formulations in fracture mechanics. *Appl. Mech. Rev.*, vol. 50, pp. 83–96.

Araujo, F. C., Mansur, W. J. and Nishikava, L. K. (2000): A linear θ time-marching algorithm in 3D BEM formulation for elastodynamics. *Eng. Anal. with Boundary Elements*, vol. 23, pp. 825–833.

Beskos, D. E. (1997): Boundary element methods in dynamic analysis: part II (1986-1996). *Appl. Mech. Rev.*, vol. 50, pp. 149–197.

Bonnet, M. (1999): *Boundary integral equation methods for solids and fluids.* John Wiley & Sons Ltd.

Chen, J. T. and Hong, H. K. (1999): Review of dual boundary element methods with emphasis on hypersingular integrals and divergent series. *Appl. Mech. Rev.*, vol. 52, pp. 17–33.

Coda, H. B. and Venturini, W. S. (1996): A smooth fundamental solution for 3D time domain BEM formulations. In: C. A. Brebbia; J. B. Martins; M. H. Aliabadi; M. Haie, M. (eds) *Boundary Elements XVIII*, Computational Mechanics Publications, Southampton.

Frangi, A. and Novati, G. (2000): On the numerical stability of time-domain elastodynamic analysis by BEM. *Comput. Meth. Appl. Mech. Eng.*, vol. 173, pp. 403–417.

Frangi, A. (2000): "Causal" shape functions in the time domain boundary element method. *Comput. Mech.*, vol. 25, pp. 533–541.

Gaul, L. and Schanz, M. (1999): A comparative study of three boundary element approaches to calculate the transient response of viscoelastic solids with unbounded domains. *Comput. Meth. in Appl. Mech. Eng.*, vol. 179, pp. 111–123.

Hwang, C. and Geubelle, P. H. (2000): A spectral scheme to simulate dynamic fracture problems in composites. *CMES: Computer Modeling in Engineering & Sciences*, vol. 1, pp. 45–56.

Kitahara, M. and Nakagawa, K. (1985): Boundary integral equations in three dimensional elastodynamics. In: *Boundary Elements VII*, Springer Verlag.

Kobayashi, S. and Nishimura, N. (1982): Transient stress analysis of tunnels and cavities of arbitrary shape due to travelling waves. In: P. K. Banerjee; R. P. Shaw (eds) *Developments in Boundary Element Methods II*, pp. 177–210. Applied Science Publishers, London.

Kögl, M. and Gaul, L. (2000): A 3-D boundary element method for dynamic analysis of anisotropic elastic solids. *CMES: Computer Modeling in Engineering & Sciences*, vol. 1, pp. 27–44.

Lubich, C. (1988a): Convolution quadrature and discretized 0perational calculus. I. *Numerische Mathematik*, vol. 52, pp. 129-145.

Lubich, C. (1988b): Convolution quadrature and discretized operational calculus. II. *Numerische Mathematik*, vol. 52, pp. 413–425.

Lubich, C. and Schneider, R. (1992): Time discretization of parabolic boundary integral equations. *Numerische Mathematik*, vol. 63, pp. 455–481.

Lubich, C. (1994): On the multistep time discretization of linear initial-boundary value problems and their boundary integral equations. *Numerische Mathematik*, vol. 67, pp. 365–389.

Lubich, C. (2000): Private communication.

Nishimura, N. and Kobayashi, S. (1989): A regularized boundary integral equation method for elastodynamic crack problems. *Comput. Mech.*, vol. 4, pp. 319–328.

Okada, H., Rajiyah, H. and Atluri, S. N. (1988): A novel displacement gradient boundary element method for elastic stress analysis with high accuracy. *ASME J. Appl. Mech.*, vol. 55, pp. 786–794.

Okada, H., Rajiyah, H. and Atluri, S.N. (1989): Non-hyper-singular integral-representations for velocity (displacement) gradients in elastic/plastic solids (small or finite deformations). *Comput. Mech.*, vol. 4, pp. 165–175.

Peirce, A. and Siebrits, E. (1997): Stability analysis and design of time-stepping schemes for general elastodynamic boundary element models. *Int. J. Numer. Meth. Engng.*, vol. 40, pp. 319-342.

Schanz, M. and Antes, H. (1997a): A new visco- and elastodynamic time domain boundary element formulation. *Computational Mechanics*, vol. 20, pp. 452-459.

Schanz, M. and Antes, H. (1997b): Application of 'operational quadrature methods' in time domain boundary element methods. *Meccanica*, vol. 32, pp. 179-186.

Schanz, M. (1998): Multistep time discretization of boundary integral equations in dynamics. In: *Modelling and Simulation Based Engineering*, S. N. Atluri; P. E. O'Donoghue (eds) vol. I, pp. 223-228, Tech Science Press.

Sládek, V. and Sládek, J. (1984): Transient elastodynamic three-dimensional problems in cracked bodies. *Appl. Math. Modelling*, vol. 8, pp. 2–10.

Tada, T., Fukuyama, E. and Madariaga, R. (2000): Non-hypersingular boundary integral equations for 3-D non-planar crack dynamics. *Comput. Mech.*, vol. 25, pp.

613–626.

Tanaka, M., Sládek, V. and Sládek J. (1994): Regularization techniques applied to boundary element methods. *Appl. Mech. Rev.*, vol. 47, pp. 457–499.

Wang, C.-C., Wang, H.-C. and Liou, G.-S. (1997): Quadratic time domain BEM formulation for 2D elastodynamic transient analysis. *Int. J. Solids Structures*, vol. 34, pp. 129–151.

Yu, G., Mansur, W. J., Carrer, J. A. M. and Gong, L. (1998a): Time weighting in time domain BEM. *Eng. Analysis with Boundary Elements*, vol. 22, pp. 175–181.

Yu, G., Mansur, W. J., Carrer, J. A. M. and Gong, L. (1998b): A linear θ method applied to 2D time-domain BEM. *Commun. Numer. Meth. Engng.*, vol. 14, pp. 1171–1179.

Yu, G., Mansur, W. J., Carrer, J. A. M. and Gong, L. (2000): Stability of Galerkin and collocation time domain boundary element methods as applied to the scalar wave equation. *Computer & Structures*, vol. 74, pp. 495–506.

Zhang, Ch. and Achenbach, J. D. (1989): A new boundary integral equation formulation for elastodynamic and elastostatic crack analysis. *ASME J. Appl. Mech.*, vol. 56, pp. 284–290.

Zhang, Ch. (1991): A novel derivation of non-hypersingular time-domain BIEs for transient elastodynamic crack analysis. *Int. J. Solids Struct.*, vol. 28, pp. 267–281.

Zhang, Ch. and Gross, D. (1992): 3-D elastodynamic crack analysis by a non-hypersingular BIEM. *Comput. Mech.*, vol. 9, pp. 137–152.

Zhang, Ch. and Gross, D. (1993): A non-hypersingular time-domain BIEM for transient elastodynamic crack analysis, *Int. J. Numer. Meth. Engng.*, vol. 36, pp. 2997-3017.

Zhang, Ch. (2000a): Transient elastodynamic antiplane crack analysis in anisotropic solids. *Int. J. Solids Structures*, vol. 37, pp. 6107–6130.

Zhang, Ch. (2000b): A 2-D time-domain BIEM for dynamic analysis of cracked orthotropic solids. In: S. N. Atluri; F. W. Brust (eds) *Advances in Computational Engineering & Sciences*, Tech Science Press, USA, vol. II, pp. 1246–1251.

Zhang, Ch. and Savaidis, A. (2000c): 3-D transient dynamic crack analysis by a novel time-domain BEM. In: S. N. Atluri; F. W. Brust (eds) *Advances in Computational Engineering & Sciences*, Tech Science Press, USA, vol. II, pp. 1240–1245.

Appendix A: Convolution quadrature formula

The Laplace transform of a function $g(t)$ is defined by

$$\hat{g}(p) = \int_0^\infty g(t)e^{-pt}dt\,, \tag{50}$$

and the inverse Laplace transform is given by

$$g(t) = \frac{1}{2\pi i}\int_{Br} \hat{g}(p)e^{pt}dp\,, \tag{51}$$

where p is a complex transform parameter and Br represents the Bromwich integration path which is an unbounded straight line parallel and right to the imaginary axis of the complex p-plane.

By using Eq. (51), the convolution integral given in Eq. (24) can be rewritten as

$$\begin{aligned} f(t) &= \int_0^t \left[\frac{1}{2\pi i}\int_{Br}\hat{g}(p)e^{p(t-\tau)}dp\right]h(\tau)d\tau \\ &= \frac{1}{2\pi i}\int_{Br}\hat{g}(p)\int_0^t e^{p(t-\tau)}h(\tau)d\tau dp\,. \end{aligned} \tag{52}$$

Introducing a function $y(t)$ as

$$y(t) = \int_0^t e^{p(t-\tau)}h(\tau)d\tau\,, \tag{53}$$

Eq. (52) can be simplified to

$$f(t) = \frac{1}{2\pi i}\int_{Br}\hat{g}(p)y(t)dp\,, \tag{54}$$

where the function $y(t)$ satisfies the following first order differential equation and the initial condition at $t = 0$

$$\dot{y}(t) = py(t) + h(t)\,, \qquad y(0) = 0\,. \tag{55}$$

A linear multistep method is applied to approximate the differential equation (55) which leads to

$$\sum_{j=0}^{k}\alpha_j y_{n-j} = \Delta t\sum_{j=0}^{k}\beta_j[py_{n-j} + h_{n-j}]\,, \quad n \geq 0 \tag{56}$$

with $y_{n-j} = y((n-j)\Delta t)$, $h_{n-j} = h((n-j)\Delta t)$, and the starting values $y_{-k} = ... = y_{-1} = 0$. Multiplying both sides of Eq. (56) by ζ^n ($|\zeta| \leq 1$), applying the following power series expressions

$$y(t) = y(\zeta) = \sum_{n=0}^{\infty} y_n \zeta^n, \qquad h(t) = h(\zeta) = \sum_{n=0}^{\infty} h_n \zeta^n, \quad (57)$$

and summing up over n from 0 to ∞ we obtain

$$y(t) = y(\zeta) = \left[\frac{\delta(\zeta)}{\Delta t} - p \right]^{-1} h(\zeta), \quad (58)$$

where the quotient of the generating polynomials of the multistep method $\delta(\zeta)$ is given by

$$\delta(\zeta) = \sum_{j=0}^{k} \alpha_j \zeta^j \Big/ \sum_{j=0}^{k} \beta_j \zeta^j. \quad (59)$$

For practical applications, we are interested in a second-order A-stable multistep method which satisfies the following conditions

$$Re[\delta(\zeta)] \geq 0, \qquad \text{for} \quad |\zeta| \leq 1, \quad (60)$$

$$\delta\left(e^{-\Delta t}\right)/\Delta t = 1 + O\left((\Delta t)^2\right), \qquad \text{for} \quad \Delta t \to 0. \quad (61)$$

It can be easily shown that the backward difference formula where $\delta(\zeta) = \sum_{j=1}^{2} (1-\zeta)^j / j$ and the trapezoidal rule with $\delta(\zeta) = 2(1-\zeta)/(1+\zeta)$ satisfy the conditions (60) and (61), and they are thus second-order A-stable methods.

Substitution of Eqs. (57) and (58) into Eq. (54) and application of the Cauchy's integral formula to Eq. (54) result in

$$f(t) = \sum_{n=0}^{\infty} f(n\Delta t)\zeta^n = \hat{g}\left(\frac{\delta(\zeta)}{\Delta t}\right) \sum_{n=0}^{\infty} h(n\Delta t)\zeta^n, \quad (62)$$

where use is made of the following asymptotic behavior of $\hat{g}(p)$

$$|\hat{g}(p)| \to 0 \qquad \text{for} \quad Re(p) \geq 0, \quad |p| \to \infty. \quad (63)$$

Substituting the power series expression for $\hat{g}(\zeta)$

$$\hat{g}\left(\frac{\delta(\zeta)}{\Delta t}\right) = \sum_{n=0}^{\infty} \omega_n(\Delta t)\zeta^n \quad (64)$$

into Eq. (62) and using Cauchy's product formula for two series, Eq. (62) can be recast into

$$\sum_{n=0}^{\infty} f(n\Delta t)\zeta^n = \sum_{n=0}^{\infty} \sum_{j}^{n} \omega_{n-j}(\Delta t) h(j\Delta t)\zeta^n. \quad (65)$$

By taking the nth coefficient of the power series of Eq. (65) we obtain finally the convolution quadrature formula (24), where the integration weights $\omega_n(\Delta t)$ are given by

$$\omega_n(\Delta t) = \frac{1}{2\pi} \int_{|\zeta|=r} \hat{g}\left(\frac{\delta(\zeta)}{\Delta t}\right) \zeta^{-n-1} d\zeta, \quad (66)$$

with r being the radius of a circle in the domain of analyticity of $\hat{g}(\zeta)$. To approximate the integral (66) with high accuracy, Lubich (1988b) suggested the following formula

$$\omega_n(\Delta t) = \frac{r^{-n}}{M} \sum_{m=0}^{M-1} \hat{g}(p_m)\Delta t \, e^{-2\pi i \cdot nm/M}, \quad (67)$$

where a trapezoidal rule with M equal steps $2\pi/M$ was used, and $p_m = \delta(\zeta_m)/\Delta t$ with $\delta(\zeta_m)$ and ζ_m being defined by Eq. (28). More details on the convolution quadrature formula can be found in Lubich (1988a,b; 1994) and Lubich and Schneider (1993).

By using Eq. (67) and

$$\hat{\hat{g}} = p^2 \hat{g}, \quad (68)$$

we obtain

$$\begin{aligned} \ddot{\omega}_n(\Delta t) &= \frac{r^{-n}}{M} \sum_{m=0}^{M-1} \hat{\hat{g}}(p_m) e^{-2\pi i \cdot nm/M} \\ &= \frac{r^{-n}}{M} \sum_{m=0}^{M-1} p_m^2 \hat{g}(p_m) e^{-2\pi i \cdot nm/M}, \end{aligned} \quad (69)$$

and this proves Eq. (41).

Substitution of the relations given in Eq. (28) and

$$\delta^2(\zeta_m) = \sum_{k=1}^{4} \delta_k^{(2)} \zeta_m^k \quad (70)$$

into Eq. (69) yields

$$\begin{aligned}
\ddot{\omega}_n(\Delta t) &= \frac{r^{-n}}{M}\sum_{m=0}^{M-1} p_m^2 \hat{g}(p_m) e^{-2\pi i\cdot nm/M} \\
&= \frac{r^{-n}}{M}\sum_{m=0}^{M-1} \frac{\delta^2(\zeta_m)}{(\Delta t)^2}\hat{g}(p_m) e^{-2\pi i\cdot nm/M} \\
&= (\Delta t)^{-2}\frac{r^{-n}}{M}\sum_{m=0}^{M-1}\left(\sum_{k=0}^{4}\delta_k^{(2)}\zeta_m^k\right)\hat{g}(p_m) e^{-2\pi i\cdot nm/M} \\
&= (\Delta t)^{-2}\sum_{k=0}^{4}\delta_k^{(2)} \\
&\quad \left[\frac{r^{-n}}{M}\sum_{m=0}^{M-1}\left(re^{2\pi i\cdot km/M}\right)^k \hat{g}(p_m) e^{-2\pi i\cdot nm/M}\right] \\
&= (\Delta t)^{-2}\sum_{k=0}^{4}\delta_k^{(2)}\left[\frac{r^{-(n-k)}}{M}\sum_{m=0}^{M-1}\hat{g}(p_m) e^{-2\pi i\cdot (n-k)m/M}\right] \\
&= (\Delta t)^{-2}\sum_{k=0}^{4}\delta_k^{(2)}\omega_{n-k}(\Delta t)\,, \qquad (71)
\end{aligned}$$

which proves Eq. (42). Note here that in deriving Eq. (71) the backward difference formula with $\delta(\zeta) = \sum_{j=1}^{2}(1-\zeta)^j/j$ has been used. If the trapezoidal rule with $\delta(\zeta) = 2(1-\zeta)/(1+\zeta)$ is applied, then Eq. (71) has to be modified properly.

Appendix B: Laplace-domain Green's functions

The Green's functions in the Laplace transform domain satisfy the following partial differential equations

$$\hat{\sigma}^G_{ijk,j} - \rho p^2 \hat{u}^G_{ik} = -\delta(\mathbf{x}-\mathbf{y})\delta_{ik}\,. \qquad (72)$$

The 3-D displacement Green's functions in the Laplace transform domain, which are solutions of the partial differential equations (72), are given by

$$\hat{u}^G_{ik}(\mathbf{x};\mathbf{y}) = \frac{k_T}{4\pi\mu}(\delta_{ik}A_1 - r_{,i}r_{,k}A_2)\,, \qquad (73)$$

where

$$\begin{aligned}
A_1 &= \left(\gamma_T^{-1}+\gamma_T^{-2}+\gamma_T^{-3}\right)\exp(-\gamma_T) \\
&- \kappa^{-3}\left(\gamma_L^{-2}+\gamma_L^{-3}\right)\exp(-\gamma_L)\,, \qquad (74)
\end{aligned}$$

$$\begin{aligned}
A_2 &= \left(\gamma_T^{-1}+3\gamma_T^{-2}+3\gamma_T^{-3}\right)\exp(-\gamma_T) \\
&- \kappa^{-3}\left(\gamma_L^{-1}+3\gamma_L^{-2}+3\gamma_L^{-3}\right)\exp(-\gamma_L)\,, \qquad (75)
\end{aligned}$$

$$\begin{aligned}
&r = |\mathbf{x}-\mathbf{y}|\,, \qquad r_i = x_i - y_i\,, \qquad r_{,i} = r_i/r\,, \\
&k_L = p/c_L\,, \qquad k_T = p/c_T\,, \qquad \kappa = k_T/k_L\,, \\
&\gamma_L = k_L r\,, \qquad \gamma_T = k_T r\,. \qquad (76)
\end{aligned}$$

By substituting Eq. (73) into Hooke's law

$$\hat{\sigma}^G_{ijk} = E_{ijmn}\hat{u}^G_{mk,n}\,, \qquad (77)$$

the corresponding stress Green's functions in the Laplace transform domain can be obtained as

$$\hat{\sigma}^G_{ijk} = \frac{k_T^2}{4\pi}\left[\delta_{ij}r_{,k}B_1 + \left(\delta_{ik}r_{,j}+\delta_{jk}r_{,i}\right)B_2 - 2r_{,i}r_{,j}r_{,k}B_3\right]\,, \qquad (78)$$

in which

$$\begin{aligned}
B_1 &= 2\left(\gamma_T^{-2}+3\gamma_T^{-3}+3\gamma_T^{-4}\right)\exp(-\gamma_T) \\
&+ \kappa^{-4}\left[\left(\kappa^2-2\right)\left(\gamma_L^{-1}+\gamma_L^{-2}\right)\right. \\
&- \left. 2\left(\gamma_L^{-2}+3\gamma_L^{-3}+3\gamma_L^{-4}\right)\right]\exp(-\gamma_L)\,, \qquad (79)
\end{aligned}$$

$$\begin{aligned}
B_2 &= \left[\gamma_T^{-1}+3\left(\gamma_T^{-2}+2\gamma_T^{-3}+2\gamma_T^{-4}\right)\right]\exp(-\gamma_T) \\
&- 2\kappa^{-4}\left(\gamma_T^{-2}+3\gamma_T^{-3}+3\gamma_T^{-4}\right)\exp(-\gamma_L)\,, \qquad (80)
\end{aligned}$$

$$\begin{aligned}
B_3 &= \left(\gamma_T^{-1}+6\gamma_T^{-2}+15\gamma_T^{-3}+15\gamma_T^{-4}\right)\exp(-\gamma_T) \\
&- \kappa^{-4}\left(\gamma_L^{-1}+6\gamma_L^{-2}+15\gamma_L^{-3}+15\gamma_L^{-4}\right)\exp(-\gamma_L)\,. \qquad (81)
\end{aligned}$$

To avoid possible cancellations in the term $[\exp(-k_T r)/r - \exp(-k_L r)/r]$ arising in the Laplace-domain Green's functions for small $k_T r$ or $k_L r$, it is convenient to use the following series expansions of the Laplace-domain Green's functions (e.g., Kobayashi and Nishimura, 1982; Kitahara and Nakagawa, 1985)

$$\hat{u}^G_{ik} = u^S_{ik} + \hat{u}^D_{ik}\,, \qquad (82)$$

where

$$u^S_{ik} = \frac{1}{8\pi\mu r}\left[\delta_{ik}\left(1+\kappa^{-2}\right)+\left(1-\kappa^{-2}\right)r_{,i}r_{,k}\right]\,, \qquad (83)$$

$$\hat{u}^D_{ik} = \frac{1}{4\pi\mu}(\delta_{ik}\Phi - r_{,i}r_{,k}\Psi)\,, \qquad (84)$$

$$\Phi = \sum_{n=1}^{\infty} \frac{(-k_T)^n}{n!} r^{n-1} - \frac{1}{k_T^2} \sum_{n=3}^{\infty} a_n (n-1) r^{n-3}, \tag{85}$$

$$\Psi = \frac{1}{k_T^2} \sum_{n=4}^{\infty} a_n (n-1)(n-3) r^{n-3}. \tag{86}$$

Substitution of Eqs. (82)–(84) into Hooke's law (77) results in

$$\hat{\sigma}^G_{ijk} = \sigma^S_{ijk} + \hat{\sigma}^D_{ijk}, \tag{87}$$

$$\begin{aligned} \sigma^S_{ijk} &= \frac{1}{4\pi(\lambda+2\mu)r^2}[\mu(\delta_{ik}r_{,j} + \delta_{jk}r_{,i} - \delta_{ij}r_{,k}) \\ &+ 3(\lambda+\mu) r_{,i} r_{,j} r_{,k}], \end{aligned} \tag{88}$$

$$\begin{aligned} \hat{\sigma}^D_{ijk} &= \frac{1}{4\pi}\{(\Psi/r - \Phi')(\delta_{ik}r_{,j} + \delta_{jk}r_{,i}) \\ &+ \left[\frac{\lambda}{\mu}(\Psi' - \Phi') + 2\left(\frac{\lambda}{\mu}+1\right)\Psi/r\right]\delta_{ij}r_{,k} \\ &+ 2(\Psi' - 2\Psi/r) r_{,i} r_{,j} r_{,k}\}, \end{aligned} \tag{89}$$

where λ and μ are Lamé's elastic constants, $\Phi' = \partial\Phi/\partial r$, $\Psi' = \partial\Psi/\partial r$, and the superscripts "*S*" and "*D*" denote the singular static Green's functions and the regular dynamic terms.

Appendix C: Conversion of surface integral

By using the definition of the 3-D Heaviside function

$$H(\mathbf{x}) = \begin{cases} 1, & \mathbf{x} \in A, \\ 0, & \mathbf{x} \notin A, \end{cases} \tag{90}$$

and the theory of generalized functions, the following identity can be obtained

$$\begin{aligned} \int_A f(\mathbf{x}) \frac{\partial H(\mathbf{x})}{\partial x_i} dS &= -\int_A H \frac{\partial f}{\partial x_i} dS \\ &= -\int_A \left(\frac{\partial f}{\partial n} - Kf\right) n_i dS - \int_{\partial A} f m_i ds, \end{aligned} \tag{91}$$

with K being the mean curvature of a sufficiently smooth surface A, $\mathbf{m} = \mathbf{t} \times \mathbf{n}$ being the unit vector normal to ∂A tangent to A and pointing outward, $\mathbf{t}$ being the unit tangent vector of ∂A (see Fig. 2), and $\partial f/\partial n$ being the derivative of f in the $\mathbf{n}$-direction. For a planar surface A lying in the x_1-x_2-plane, $K = \partial f/\partial n = 0$, and Eq. (91) is simplified to

$$\int_A f(\mathbf{x}) \frac{\partial H(\mathbf{x})}{\partial x_i} dS = -\int_{\partial A} f m_i ds. \tag{92}$$